Faraday Discussions

Cite this: *Faraday Discuss.*, 2016, **188**, 309

Supports and modified nano-particles for designing model catalysts

C. P. O'Brien,[a] K.-H. Dostert,[b] M. Hollerer,[c] C. Stiehler,[b] F. Calaza,[b] S. Schauermann,[bd] S. Shaikhutdinov,[b] M. Sterrer[c] and H.-J. Freund*[b]

Received 9th October 2015, Accepted 21st October 2015
DOI: 10.1039/c5fd00143a

In order to design catalytic materials, we need to understand the essential causes for material properties resulting from its composite nature. In this paper we discuss two, at first sight, diverse aspects: (a) the effect of the oxide–metal interface on metal nanoparticle properties and (b) the consequences of metal particle modification after activation on the selectivity of hydrogenation reactions. However, these two aspects are intimately linked. The metal nanoparticle's electronic structure changes at the interface as a catalyst is brought to different reaction temperatures due to morphological modifications in the metal and, as we will discuss, these changes in the chemistry lead to changes in the reaction path. As the morphology of the particle varies, facets of different orientations and sizes are exposed, which may lead to a change in the surface chemistry as well. We use two specific reactions to address these issues in some detail. To the best of our knowledge, the present paper reports the first observations of this kind for well-defined model systems. The changes in the electronic structure of Au nanoparticles due to their size and interaction with a supporting oxide are revealed as a function of temperature using CO_2 activation as a probe. The presence of spectator species (oxopropyl), formed during an activation step of acrolein hydrogenation, strongly controls the selectivity of the reaction towards hydrogenation of the unsaturated C=O bond *vs.* the C=C bond on Pd(111) when compared with oxide-supported Pd nanoparticles.

Introduction

The properties of dispersed metal catalysts are dominated by two factors: the size, morphology, and chemical modification of the metal nanoparticles after having been activated, and the interaction of these nanoparticles, or small metal clusters, with the support, *i.e.* the metal–support interface. These two factors are strongly

[a]*US Army Research Laboratory, USA*
[b]*Fritz Haber Institute of the Max Planck Society, Department of Chemical Physics, Faradayweg 4-6, 14195 Berlin, Germany. E-mail: freund@fhi-berlin.mpg.de*
[c]*Institute of Physics, University of Graz, Austria*
[d]*Institut für Physikalische Chemie, Christian-Albrechts-Universität zu Kiel, Germany*

interlinked and need to be addressed in model studies if we want to understand their influence at the atomic level and find design principles for new catalytic materials. This is described in this paper and exemplified by investigating two, seemingly different, model systems.

There is no doubt that the metal–support interface is one of the determining factors in catalysis, as documented by many examples in the literature,[1] yet, it is not considered in most model studies. The electronic structure of the metal–support interface changes as the morphology of the metal particle may vary as a function of temperature, for example, due to sintering. This may lead to the formation of particles with a variety of facets, which, in turn, changes the surface chemistry.[2–5]

Plausible explanations have been presented over the years for the "structure sensitivity", defined early on by Michel Boudart in connection with the function of the catalyst. It mainly refers to the size of a metal nanoparticle and relates to the various possible terminations with different facets.[4–6] This concept was taken as a basis for the surface science approach based on metal single crystal surfaces with respect to experiments,[7,8] and theoretical slab calculations,[9] with varying terminations, the result of which could be used by superposition to explain the observed catalytic behavior. While in this approach the support might be taken as the cause of the particular appearance of the nanoparticle, the support's chemical nature and specific interaction with the nanoparticle are not taken into account in such approaches.[10] The appearance of particles of different sizes and shapes may cause a modification of the catalyst during the activation process. A series of attempts has been made in the literature to consider material modification by the overgrowth of oxide films[11] or the incorporation of carbon in the surface[2] as well as subsurface areas, which only then is turned into an effective hydrogenation catalyst.[12] Robert Schlögl[13] has recently presented a comprehensive review on the dynamic catalyst.

In the present paper we would like to address both the influence of the metal–oxide interface, as well as the influence of spectator species on selective hydrogenation, in an attempt to exemplify design principles for new catalytic materials. The present work is based on and is a substantial extension of previous work on CO_2 activation on supported Au nanoparticles and on the competitive, selective hydrogenation of C=C *vs.* C=O double bonds on oxide-supported Pd nanoparticles as a function of particle size. The paper is organized as follows: after a short description of the experiments, we present and discuss the new results in comparison to the results obtained so far. We conclude with a summary and an outlook to further experiments.

Experimental conditions

The experiments on supported Au nanoparticles on ultrathin MgO(100) films were carried out using different ultrahigh-vacuum (UHV) set-ups, all of them equipped with basic sample cleaning and preparation (sputtering, heating, evaporation, gas dosing) as well as characterization (low-energy electron diffraction, LEED) facilities. One of them had, in addition, a polarization modulation infrared reflection absorption spectroscopy (IRAS) and X-ray photoelectron spectroscopy (XPS) set-up attached. Infrared spectra were acquired with a Bruker IFS66v FTIR spectrometer using a liquid nitrogen cooled MCT detector. The XPS

spectrometer was a SPECS type hemispherical analyzer (Phoibos 150) with a dual anode (Mg/Al) X-ray source. Scanning tunneling microscopy (STM) experiments were carried out both at the Fritz Haber Institute using a home-built low-temperature STM operated at liquid helium temperature as well as in the Physics Department of the University of Graz using a CreaTec low-temperature STM operated at liquid nitrogen temperature. The surface of the Ag(100) crystal used as a support for the MgO(100) films was cleaned by repeated sputter (Ar^+, 800 V, 5 μA)–anneal (700 K) cycles, and the cleanliness and surface quality was checked using LEED, as well as Auger spectroscopy and XPS. Preparation of the MgO films was carried out according to published methods by reactive deposition of Mg in an oxygen atmosphere (1×10^{-6} mbar).[14] CO_2 was dosed from the background *via* a leak valve.

The experiments on acrolein hydrogenation on iron oxide supported Pd were performed with an ultra-high vacuum molecular beam machine that has been described in detail previously.[15] Molecular beams of acrolein and H_2 were directed at the sample simultaneously while the sample was held at a constant temperature. The effusive molecular beams were produced by doubly differentially pumped multi-channel array sources. Acrolein (Sigma-Aldrich, 95% purity) was purified prior to each experiment by repeated freeze–pump–thaw cycles. During all reactivity experiments the flux of H_2 on the sample surface was 4.8×10^{15} molecules per cm^2 per s. The sample was exposed to H_2 for five minutes prior to acrolein exposure. The flux of acrolein on the sample surface was 1.5×10^{13} molecules per cm^2 per s. Gas-phase fragments $m/z = 56$, 57, and 58 were detected with a quadrupole mass spectrometer (QMS) (ABB Extrel). Acrolein and the hydrogenation products propenol and propanal were identified by their fragmentation patterns in the QMS. Acrolein generates signals at $m/z = 56$, 57, and 58 with an intensity distribution of 1 : 0.04 : 0.01. Propenol causes signals at $m/z = 57$ and 58 with an intensity ratio of 1 : 0.1, and propanal was identified by signals at the same masses with an intensity distribution of 0.3 : 1. Surface species were detected simultaneously with the gas-phase products using an infrared spectrometer (Bruker IFS 66v) with an MCT detector and a spectral resolution of 2 cm^{-1}.

A well-ordered ~10 nm thick Fe_3O_4 film was grown on a Pt(111) substrate (see ref. 16 and 17 for details), followed by Pd deposition onto the Fe_3O_4 film at 120 K by physical vapor deposition of Pd (Goodfellow, >99.9%) using a commercial evaporator (Focus EFM 3). After depositing Pd, the sample was annealed at 600 K and the Pd nanoparticles were stabilized by repeated cycles of oxidation and reduction at 500 K.[18] The size of the Pd nanoparticles was controlled by the nominal thickness of the Pd film deposited onto the Fe_3O_4 substrate at 120 K, in comparison with the STM images reported previously (see ref. 19 for details). The Pd(111) crystal was cleaned by repeated cycles of Ar^+ sputtering at room temperature, annealing at 1000 K, and oxidation in 1×10^{-6} mbar O_2 at 750 K. The cleanliness of the Pd/Fe_3O_4 and Pd(111) samples was verified prior to every experiment by infrared reflection absorption spectroscopy (IRAS) of adsorbed CO.

Results and discussion

Activation of carbon dioxide[20,21]

In a previous study[21] we observed a scenario schematically represented in Fig. 1. A two-layer MgO film was grown on an Ag(100) substrate, and Au was deposited

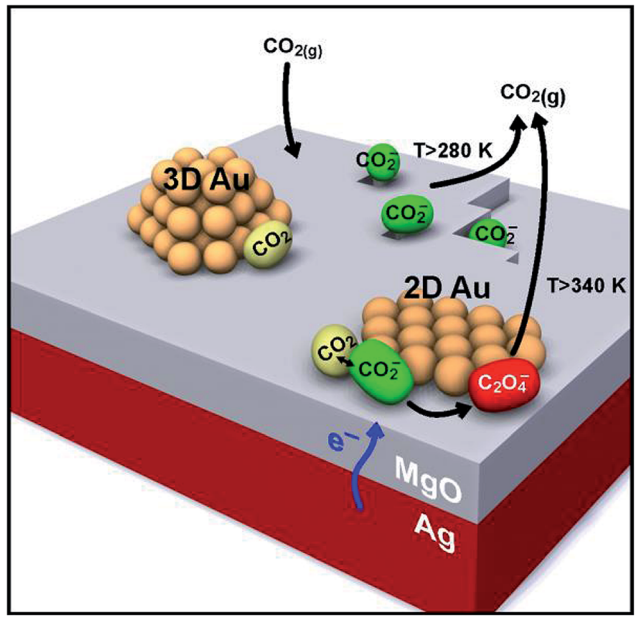

Fig. 1 Schematic showing the individual steps of oxalate formation upon chemisorption of CO_2 on the rim of 2D Au islands on thin MgO(001)/Ag(001) films.[21] Carboxylate species (green) are formed both on defect sites of the MgO film and on the rim of the 2D Au islands by electron transfer. Only on the latter, is additional CO_2 (yellow) able to solvate the carboxylate species, yielding a $(CO_2)_2^-$ dimer ion, which, after an additional electron transfer, results in adsorbed oxalate $C_2O_4^{2-}$ (red). This reaction does not occur on 3D Au particles.

from an Au evaporator at 77 K, and annealed consecutively at 300 K. It was noticed previously that deposition at a low temperature led to the two-dimensional growth of Au nanoparticles and islands,[22] as suggested by theoretical calculations.[23] The driving force for this unusual wetting of the oxide surface is an electron transfer from the Ag substrate through the film and collected by the Au islands due to the large electron affinity of Au.[23] STM investigations, together with model calculations, suggested that the charge in this metal–insulator–metal (MIM) system localizes at the rim of the nanoparticles, *i.e.* at the nanoparticle–oxide interface.[24] Having noticed this phenomenon, a study of the molecular adsorption was started. The first attempt was made using CO.[25] However, it turned out that direct imaging of the molecules was not possible, but inelastic spatially resolved electron tunneling spectra of the CO hindered translation at 45 meV provided evidence that these molecules do interact exclusively with the rim of the nanoparticle. It is interesting to note that the CO molecules do not exhibit an appreciable IR intensity.[25] This is indicative of a geometry leading to a small dipole moment perpendicular to the surface. Following up on this, we investigated the adsorption of a bigger molecule, isophorone, promising easier constant current imaging. It was possible to image the molecule at the rim, and, in addition, to study the consequences of adsorption on the quantum well states of the nanoparticle, which develop due to its finite size.[26] In fact, the energetic position of the quantum well states of the same nanoparticle was compared with those of the

particle interacting with isophorone. Isophorone, as revealed by infrared spectroscopy, physisorbs on Au nanoparticles. This leads to a characteristic enhancement of the effective electron mass of the Au electrons, in line with physisorption. While this is important to understand the details of the molecule–nanoparticle interaction, these observations do not provide evidence for a reaction. This came from studies of CO_2 adsorption on these systems.[21] When CO_2 adsorbs on the surface, it is located at the rim of the clusters and it transforms to CO_2^- (see Fig. 1) by electron transfer from the Au nanoparticle. While this process is energetically uphill by 0.6 eV, the presence of additional CO_2, able to "solvate" the carboxylate to a $(CO_2)_2^-$ dimer ion, leads to a 1.6 eV downhill process. Spectroscopic studies, further elaborated and extended on below, suggest, together with model calculations, that this finally results in an oxalate ion by a second electron transfer, all happening at the rim of the nanoparticle.

Fig. 2 shows a set of infrared spectra of the surface as a function of annealing temperature. First, we concentrate on the trace recorded at the lowest temperature. The peak at 1295 cm^{-1} is due to CO_2 adsorption on the oxide support forming a carboxylate, *i.e.* not a carbonate(!), at specific sites on the MgO film. The two bands at 1220 cm^{-1} and 1440 cm^{-1} have been identified as being due to the oxalate species. This spectrum is entirely consistent with the spectra recorded before.[21] The other spectra in Fig. 2 have been recorded after annealing the Au

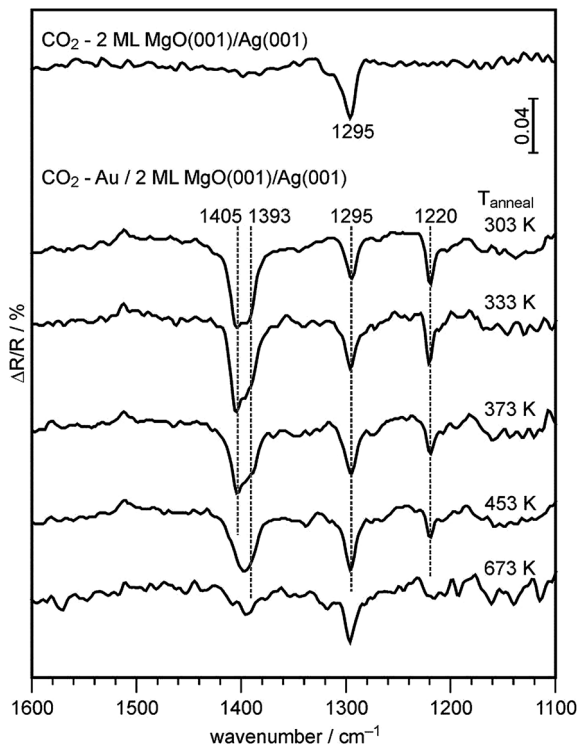

Fig. 2 IRA spectra of bare (top) and Au-loaded 2 monolayer (ML) thick MgO(001)/Ag(001) samples recorded after a saturation dose of CO_2 at 223 K. Au was deposited at 100 K and the samples were subsequently annealed at the indicated temperature prior to CO_2 adsorption.

deposits at higher temperatures. Obviously, annealing at a higher temperature does not influence the intensities in the infrared spectra massively, unless the system is annealed at or higher than 500 K. This is also consistent with our previous findings using temperature programmed desorption, where oxalate dissociation into two CO_2 molecules started to occur well below this temperature. If one annealed not quite at this temperature, then the process of oxalate formation was entirely reversible. This hinted towards a kinetically controlled process that changes the system.

Ricci *et al.*,[23] in a landmark paper, demonstrated that for nanoparticles on ultrathin oxide films, the electron transfer through the film depends strongly on the dimensionality of the Au particle on the oxide. Clearly, a two-dimensional particle was prone to accepting more electronic charge than a three-dimensional particle, and it also depended considerably on the contact area of the particle. Given this scenario, one might envision that by increasing the mobility of the Au atoms on the oxide film through annealing at a higher temperature, three-dimensional particles start to grow on the film. These particles would exhibit a small enough charge transfer that the chemical potential for forming the CO_2 anion and the oxalate is impossible. This would establish the first proof of a morphology driven change in a reaction at the oxide metal interface. In order to see whether this would be a valid interpretation, we performed and present here a STM study that is summarized in Fig. 3. This figure shows a set of STM images taken at different annealing temperatures. Fig. 3a has been recorded at 77 K and reveals Au adsorbed as single atoms or small clusters. Annealing at room temperature or slightly above (Fig. 3b) causes two-dimensional islands to form all over the surface. Their average size varies between 3 and 5 nm with a variation in shape ranging from roundish (hexagonal) islands to more rectangular (raft-like) ones. This is consistent with our previous findings.[22] Increasing the temperature to 400 K increases the average island diameter to 4–8 nm but does not change the growth mode (Fig. 3c). A drastic change occurs if the annealing temperature is raised to 500 K (Fig. 3d). We find a cross-over to three-dimensional growth with particle diameters between 5 and 10 nm, and heights of 1–2 nm. There are still a few two-dimensional islands observed, but most of the Au is contained in 3D particles.

Using this information we may now return to a discussion of Fig. 2, and try to understand the changes in the oxalate signals as a function of temperature. As stated above, the lowest temperature trace represents the oxalate species at the rim of the 2D nanoparticles, as proven in previous reports.[21] The infrared spectra start to attenuate and significantly change after the system has been either prepared at temperatures higher than approx. 500 K, or annealed for a sufficiently long time at that temperature. We know from the above STM study that this is concomitant with the change from 2D to 3D morphology. As referred to above, the formation of the 3D particles reduces the electron transfer from the Ag substrate, and, we conclude, must be the reason for the reduced ability to form oxalate species. Note that the species due to adsorption on the MgO film at 1295 cm^{-1} is not influenced by the change in growth mode.

At the present time, theoretical modeling of the process, which would be highly desirable, is not possible. Hannu Häkkinen and his group have greatly contributed to our understanding of the oxalate formation, as documented in ref. 21. However, a full, detailed description involving nanoparticles of the size observed experimentally seems to be out of range at present. Schematically, as

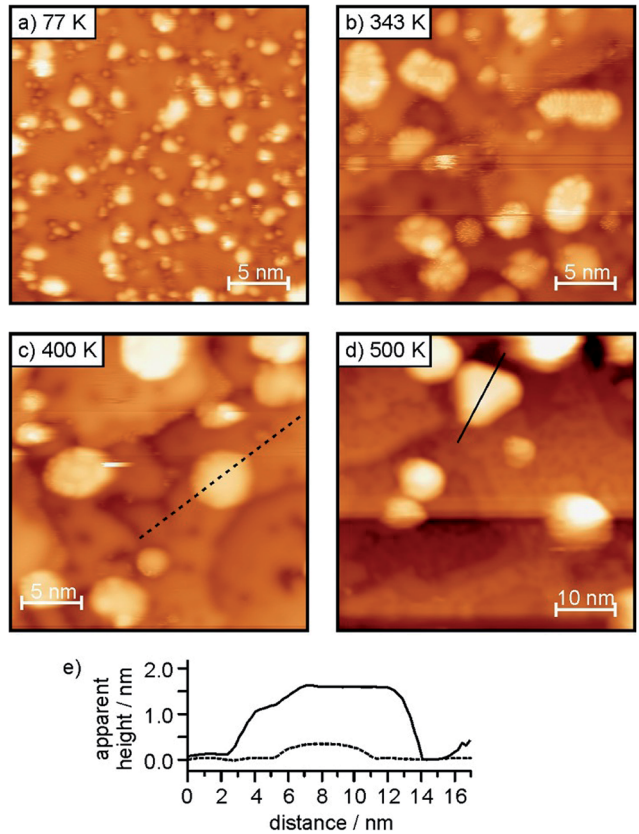

Fig. 3 STM images of (a) Au deposited on 2 ML MgO(001)/Ag(001) at 77 K, and after subsequent annealing of the system at 343 K (b), 400 K (c) and 500 K (d). All images were taken at 77 K. Scan area: (a)–(c) 25 nm × 25 nm; (d) 50 nm × 50 nm. $U_{bias} = +(0.5–0.75)$ V. $I_t = 30$ pA. (e) Height profiles of representative islands/particles from the 400 K (dashed line) and 500 K (solid line) annealed samples, highlighting the transition from 2D to 3D geometries.

depicted in Fig. 1, this means a change from reacting CO_2 at nanoparticles (2D) towards unreactive particles with a 3D morphology. To the best of our knowledge, this is the first clear experimental indication for such behavior.[27]

In order to relate the findings reported in this paper to the design of real powder-based catalysts, we refer to our study showing doping of bulk oxides with transition metals,[28] which provide an electron source to trigger a similar control of morphology as the Ag support of the ultrathin film. It will be a future task to experimentally establish this in model systems and in powder samples. However, based on the findings reported here, one may envision the control and design of CO_2 activation catalysts by doping induced charge transfer, and thus this establishes a design principle for supported Au catalysts.

Hydrogenation of acrolein[29]

Hydrogenation of C=C double bonds has been shown to depend on the presence of hydrogen atoms absorbed inside the metal nanoparticles.[2] The absorbed

hydrogen provides a pool to sustain catalytic activity. Carbon and/or carbonaceous deposits adsorbed at the particle's corners and edges control the diffusion of the hydrogen necessary for hydrogenation from below the surface to the surface of the particle. The selective, competitive hydrogenation of acrolein, *i.e.* the hydrogenation of a C=C double bond *versus* the hydrogenation of a C=O double bond, represents an even more ambitious situation.[29]

In a previous study,[29] we investigated the selectivity of the partial hydrogenation of acrolein on a Pd(111) single crystal and on Pd/Fe_3O_4 model catalysts by isothermal molecular beam experiments under well-defined UHV conditions. The formation of gas-phase products was detected by quadrupole mass spectrometry (QMS); simultaneously, the evolution of surface species was investigated by infrared reflection absorption spectroscopy (IRAS) studies. Pd(111) and Pd/Fe_3O_4 showed very different selectivities in the partial hydrogenation of acrolein. Over Pd/Fe_3O_4, selective conversion of acrolein to propanal occurs, while over a Pd(111) single crystal, propenol is formed with near 100% selectivity. IRAS studies on the surface turning over showed that the selectivity for propenol formation on Pd(111) critically depends on the presence of a dense overlayer of an oxopropyl species formed at an initial stage of acrolein and hydrogen exposure. On the modified Pd(111) surface, acrolein is adsorbed *via* the C=O bond and reacts with propenol. On Pd/Fe_3O_4, however, significantly different surface chemistry occurs under identical experimental conditions. Instead of forming an oxopropyl layer, a fraction of the acrolein molecules decomposes, forming CO molecules and C_xH_y fragments that eventually block all Pd sites, while the propanal formation rate decreases to zero. Most likely, low-coordinated surface sites and (100) facets of the Pd clusters are responsible for the rapid acrolein decarbonylation. The reason for the significantly different surface chemistry on Pd/Fe_3O_4 and Pd(111), however, needs further investigation. In particular, a detailed kinetic analysis of all possible reaction pathways on the different Pd surfaces would be required. Nevertheless, our investigations unambiguously show that the modification of the Pd(111) surface with a dense oxopropyl overlayer correlates with a change in selectivity from propanal to propenol formation. Moreover, the absence of the oxopropyl layer on Pd/Fe_3O_4 seems to be related to the decarbonylation of acrolein.

Based on our previous results, we have addressed the question of whether it is possible to also produce propenol on Pd/Fe_3O_4 model catalysts. We could think about a large number of different approaches, such as modifying the Pd clusters prior to acrolein conversion, *e.g.* by pre-adsorbed CO or hydrocarbons or by C modification of low-coordinated Pd sites. In the present study, however, we focus on the effect of Pd particle size. We have investigated the hydrogenation of acrolein on 7 nm and 12 nm Pd particles using molecular beam techniques under isothermal conditions. The formation of the gas-phase products has been detected by QMS and the surface composition has been simultaneously investigated by IRAS. In all experiments, the surface was pre-exposed to 4.8×10^{15} H_2 per cm^2 per s for 300 s before the acrolein beam with 1.5×10^{13} molecules per cm^2 per s was switched on.

Fig. 4 shows the formation rates of the partial hydrogenation products on Fe_3O_4-supported 7 nm and 12 nm Pd particles detected in the gas phase. With both particles sizes, similar propanal formation rates are observed, which pass through a maximum after about 30 s and then decrease to zero. On the 12 nm

particles, however, a small amount of propenol is also detected. The propenol production rate rapidly increases after about 40 s, when the propanal formation has almost stopped, passes through a maximum after about 60 s and finally decreases to zero. In general, both partial hydrogenation products have been identified by their characteristic fragmentation patterns in QMS. The clearly different time dependence of the two product formation rates in this study, however, provides an additional possibility to unambiguously distinguish between propanal and propenol. Nevertheless, the total amount of propenol that is formed on the 12 nm particles is much smaller than on a Pd(111) single crystal. It should be noted that the formation of gas-phase propenol has only been detected in a narrow temperature range near 250 K. It was not observed in our previous studies on Pd particles under slightly different conditions, such as a lower or higher surface temperature or when using a pulsed acrolein beam instead of continuous exposure.

Fig. 5 illustrates the correlation between the evolution of propenol in the gas phase detected by QMS and the formation of surface species on the 12 nm Pd particles turning over, as studied by IRAS. A time-dependent series of IR spectra obtained with a time resolution of 45 s is shown in Fig. 5a. IR absorption features appear near 1855 cm^{-1}, 1755 cm^{-1}, and 1670 cm^{-1}. The vibration at 1670 cm^{-1} is most likely associated with the C=O stretching in molecularly adsorbed acrolein. It has been assigned to acrolein adsorbed on a Pd(111) single crystal in a previous study.[29] The adsorbate giving rise to the IR absorption near 1755 cm^{-1} accumulates at the beginning of the acrolein exposure and saturates during the first 45 s. Interestingly, this band has previously been related to the oxopropyl species modifying the Pd(111) surface for propenol production. The IR vibration at 1855 cm^{-1} most likely shows CO adsorbed on the Pd(111) facets. The slowly increasing IR absorption intensity indicates a rather slow accumulation of CO, most likely from acrolein decarbonylation. Hence, the decarbonylation of acrolein is significantly less efficient at 250 K compared to our previous studies at 270 K. Fig. 5b illustrates the simultaneously recorded propenol evolution in the gas phase. A

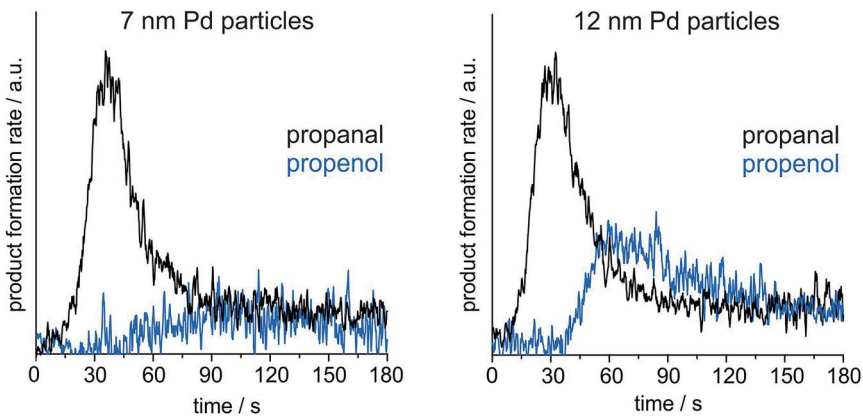

Fig. 4 Formation rates of propanal (black lines) and propenol (blue lines) over Fe_3O_4-supported Pd particles with diameters of 7 nm (left) and 12 nm (right) at 250 K, detected by QMS.

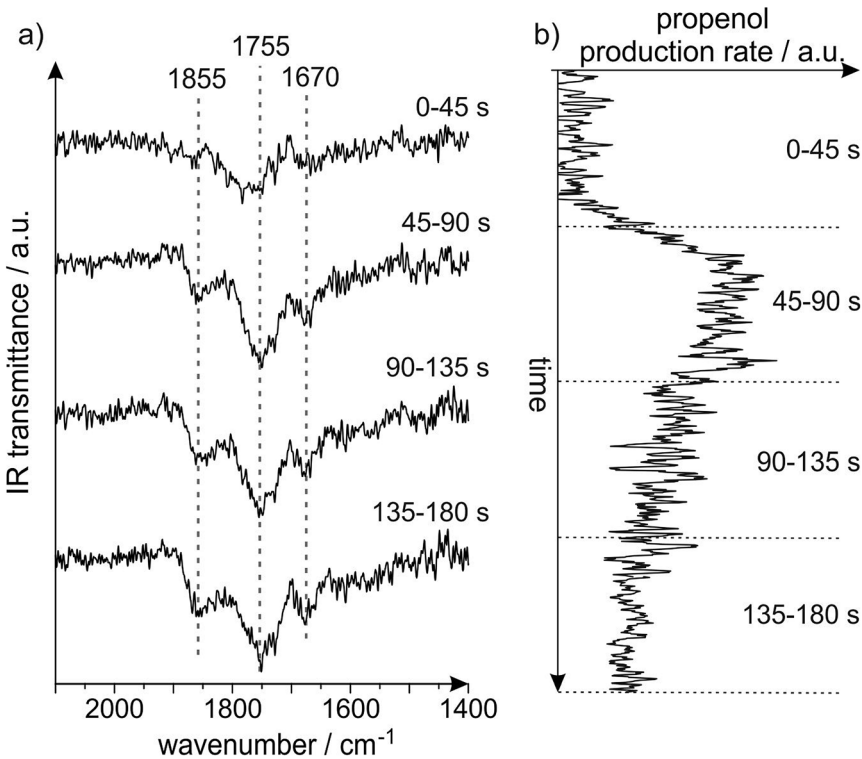

Fig. 5 (a) Time-resolved IR spectra monitoring the evolution of surface species on the 12 nm Pd particles turning over and (b) QMS measurements showing the formation rate of propenol in the gas phase.

clear onset is observed after about 40 s, which is approximately when the oxopropyl species saturates.

The simultaneously performed IRAS and QMS studies on the 12 nm Pd particles turning over at 250 K give detailed insights into the mechanism of the acrolein conversion. On the one hand, our results strongly reveal that on the 12 nm particles a modification of the surface by an oxopropyl layer triggers the propenol production. In contrast to Pd(111), however, the additional presence of acrolein and CO on the surface reveals that the oxopropyl species is not covering the whole Pd surface with a dense layer. On the other hand, it is again indicated that the decarbonylation of acrolein has to be avoided to form propenol on Pd particles. By reducing the surface temperature from 270 K to 250 K, the decarbonylation of acrolein is largely suppressed, while the temperature is still high enough to form a small amount of propenol. It seems that the temperature needs to be carefully chosen to keep the decarbonylation reaction rate as low as possible, while the propenol formation rate should still be sufficiently high.

Our studies show a significant particle size dependence of the selectivity in the partial hydrogenation of acrolein over Pd model catalysts at 250 K. On both 7 nm and 12 nm Pd particles, a similar amount of propanal is formed. Hydrogenation of acrolein to propenol, in contrast, appears possible only on 12 nm particles. The clearly different time dependence of propanal and propenol evolution agrees well

with our previous findings, showing propanal formation as long as pristine Pd is available and propenol production, in contrast, after a dense oxopropyl overlayer is formed. It seems that the selectivity towards propenol formation increases with increasing Pd cluster size from 0% on 7 nm Pd particles and a small amount over 12 nm Pd particles to approximately 100% on a Pd(111) single crystal. Possibly, the formation of an oxopropyl layer on sufficiently large domains is necessary to produce propenol, which is more likely to happen on larger Pd clusters having larger (111) facets and a lower concentration of low-coordinated sites. Low-coordinated sites, such as edges, corners, and defects, may catalyze acrolein decarbonylation.

Synopsis

The present study clearly points to two important factors influencing the catalytic activity of supported metal nanoparticles, which influence the design of new catalytic materials:

• The interaction with the support controls the size and shape of the nanoparticle, and, in particular, the charge exchange and transfer at the oxide–metal interface. Specifically designed model systems allow us to isolate details of the problem and study them at the atomic level. Here, the surface science approach turns out to be the method of choice to image and characterize molecules interacting with the metal particle at the metal–oxide interface using a combination of scanning probe and spectroscopic techniques. This has allowed, for the first time, the direct identification of the consequence of molecular adsorption and reaction on the electronic structure of a metal nanoparticle. Temperature is decisive in determining the mobility of metal atoms and particles on supports. We show in this paper that a change in particle morphology controls the reactivity of the system at the oxide–metal interface, as the transition from two-dimensional Au particles at a lower temperature to three-dimensional growth at a higher temperature reduces the charge transfer from the support to the metal nanoparticle.

• Adsorbed species formed during a reaction, which are not turned over, have been identified as being able to modify a supported metal nanoparticle, and *via* this modification, control the selectivity of a hydrogenation reaction. The selective hydrogenation of acrolein has been studied as an example. In particular, an oxopropyl species formed from adsorbed acrolein modifies the surface in such a way that acrolein hydrogenation leads to propenol and the hydrogenation of the C=C double bond is avoided. We have demonstrated before that Pd(111) single crystals selectively hydrogenate the C=O bond in acrolein, while supported Pd nanoparticles exclusively hydrogenate the C=C bond. We show in this paper that there is a particle size effect. The particle needs to have a certain size in order to expose (111) facets of a sufficient size to favor the effect. If particles are smaller, presumably the presence of edges, corners and irregularities in the particles favor the formation of CO, which poisons the oxopropyl effect.

The knowledge derived from both of these observations can be used to design catalytic materials and control catalytic reactions.

Acknowledgements

We are grateful to the German Science Foundation through the cluster of Excellence Unicast (administered by the TU Berlin) as well as the Fonds der

Chemischen Industrie for financial support. F. Calaza thanks the Alexander von Humboldt foundation for a Georg Forster Research Fellowship. C. Stiehler thanks the Studienstiftung des Deutschen Volkes for a fellowship. S. Schauermann is grateful to the European Research Council for a Starting Grant "Enantioselective Reactions on Model Chirally Modified Surfaces". M. Sterrer acknowledges support from the European Research Council through Grant Agreement No. 280070 (STRUBOLI).

References

1 H. K. G. Ertl, F. Schüth and J. Weitkamp, *Handbook of Heterogeneous Catalysis*, VCH, Wiley-VCH, Weinheim, compl. rev. and enlarged ed. edn., 2008.
2 M. Wilde, K. Fukutani, W. Ludwig, B. Brandt, J.-H. Fischer, S. Schauermann and H. J. Freund, *Angew. Chem., Int. Ed.*, 2008, **47**, 9289–9293.
3 S. J. Thomson and G. Webb, *J. Chem. Soc., Chem. Commun.*, 1976, 526–527.
4 G. C. Bond, *Metal-Catalysed Reactions of Hydrocarbons*, Springer, US, New York, 2005.
5 J. Sauer and H.-J. Freund, *Catal. Lett.*, 2015, **145**, 109–125.
6 M. Boudart and G. Djéga-Mariadassou, *La cinétique des réactions en catalyse hétérogène*, Masson, Paris, New York, 1982.
7 G. Ertl, *Angew. Chem., Int. Ed.*, 2008, **47**, 3524–3535.
8 G. Ertl and H. J. Freund, *Phys. Today*, 1999, **52**, 32–38.
9 J. Sauer, *Chem. Rev.*, 1989, **89**, 199–255.
10 H. J. Freund, N. Nilius, T. Risse and S. Schauermann, *Phys. Chem. Chem. Phys.*, 2014, **16**, 8148–8167.
11 S. Shaikhutdinov and H.-J. Freund, *Annu. Rev. Phys. Chem.*, 2012, **63**, 619–633.
12 D. Teschner, J. Borsodi, A. Wootsch, Z. Révay, M. Hävecker, A. Knop-Gericke, S. D. Jackson and R. Schlögl, *Science*, 2008, **320**, 86–89.
13 R. Schlögl, *Angew. Chem., Int. Ed.*, 2015, **54**, 3465–3520.
14 J. Pal, M. Smerieri, E. Celasco, L. Savio, L. Vattuone and M. Rocca, *Phys. Rev. Lett.*, 2014, **112**, 126102.
15 J. Libuda, I. Meusel, J. Hartmann and H.-J. Freund, *Rev. Sci. Instrum.*, 2000, **71**, 4395.
16 W. Weiss and W. Ranke, *Prog. Surf. Sci.*, 2002, **70**, 1–151.
17 C. Lemire, R. Meyer, V. E. Henrich, S. Shaikhutdinov and H. J. Freund, *Surf. Sci.*, 2004, **572**, 103.
18 T. Schalow, B. Brandt, D. Starr, M. Laurin, S. Schauermann, S. Shaikhutdinov, J. Libuda and H. J. Freund, *Catal. Lett.*, 2006, **107**, 189–196.
19 T. Schalow, B. Brandt, D. E. Starr, M. Laurin, S. K. Shaikhutdinov, S. Schauermann, J. Libuda and H. J. Freund, *Phys. Chem. Chem. Phys.*, 2007, **9**, 1347–1361.
20 H.-J. Freund and M. W. Roberts, *Surf. Sci. Rep.*, 1996, **25**, 225–273.
21 F. Calaza, C. Stiehler, Y. Fujimori, M. Sterrer, S. Beeg, M. Ruiz-Oses, N. Nilius, M. Heyde, T. Parviainen, K. Honkala, H. Häkkinen and H.-J. Freund, *Angew. Chem., Int. Ed.*, 2015, **54**, 12484.
22 M. Sterrer, T. Risse, U. Martinez Pozzoni, L. Giordano, M. Heyde, H.-P. Rust, G. Pacchioni and H.-J. Freund, *Phys. Rev. Lett.*, 2007, **98**, 096107.
23 D. Ricci, A. Bongiorno, G. Pacchioni and U. Landman, *Phys. Rev. Lett.*, 2006, **97**, 036106.

24 X. Lin, N. Nilius, M. Sterrer, P. Koskinen, H. Haekkinen and H.-J. Freund, *Phys. Rev. B: Condens. Matter Mater. Phys.*, 2010, **81**, 153406.
25 X. Lin, B. Yang, H. M. Benia, P. Myrach, M. Yulikov, A. Aumer, M. Brown, M. Sterrer, O. Bondarchuk, E. Kieseritzky, J. Rocker, T. Risse, H. Gao, N. Nilius and H. J. Freund, *J. Am. Chem. Soc.*, 2010, **132**, 7745–7749.
26 C. Stiehler, F. Calaza, W.-D. Schneider, N. Nilius and H.-J. Freund, *Phys. Rev. Lett.*, 2015, **115**, 036804.
27 M. Chen and D. W. Goodman, *Chem. Soc. Rev.*, 2008, **37**, 1860–1870.
28 X. Shao, S. Prada, L. Giordano, G. Pacchioni, N. Nilius and H.-J. Freund, *Angew. Chem., Int. Ed.*, 2011, **50**, 11525–11527.
29 K.-H. Dostert, C. P. O'Brien, F. Ivars-Barcelo, S. Schauermann and H.-J. Freund, *J. Am. Chem. Soc.*, 2015, **137**, 13496–13502.